J. Environ. Nanotechnol.
Volume 3, No.2 pp. 130-149
ISSN (Print) : 2279-0748
ISSN (Online) : 2319-5541
doi : 10.13074/jent.2014.03.143083

The Spectroscopic Investigation of 3-amino-2-pyrazine carboxylic acid and methyl-3-amino-2-pyrazine carboxylate – A Comparative Study

N. Prabavathi[1*], A. Nilufer[2]

Department of Physics, Sri Sarada College for women (Autonomous), Salem, TN, India.

Received : 18.04.2014 Accepted : 30.05.2014

Abstract

The FTIR and FT-Raman spectra of 3-amino-2-pyrazine carboxylic acid (APC) and methyl-3-amino-2-pyrazine carboxylate (MAPC) have been recorded in the region 4000–400 cm^{-1} and 3500–100 cm^{-1} respectively. The optimized geometry, frequency and intensity of the vibrational bands of the compounds were obtained by the density functional theory using 6–311++G(d,p) basis set. The harmonic vibrational frequencies were calculated and the scaled values have been compared with experimental FTIR and FT-Raman spectra. The observed and the calculated frequencies are found to be in good agreement. A detailed interpretation of the infrared and Raman spectra were also reported based on potential energy distribution (PED). ^{1}H and ^{13}C NMR spectra were recorded and its corresponding nuclear magnetic resonance chemical shifts of the molecule were also calculated using the gauge independent atomic orbital (GIAO) method. UV–Visible spectrum of these compounds was recorded and the electronic properties HOMO and LUMO energies were measured by TD–DFT approach. The calculated HOMO and LUMO energies show that charge transfer occurs within the molecule. Furthermore, molecular electrostatic potential was performed. Molecular stability and bond strength were investigated by applying the natural bond orbital analysis (NBO).

Keywords: *Frontier molecular orbitals; FTIR; FT-Raman spectra; methyl-3-amino-2-pyrazinecarboxylate; 3-amino-2-pyrazinecarboxylicacid.*

1. INTRODUCTION

Pyrazine and its derivatives are very important to consider among N-heterocycles. Pyrazine is a building block of phenazine and pteridines. They are present in natural flavours and complex organic molecules and present in many compounds with pharmaceutical and flavouring applications (Chacko Yohannan Panickar *et al*. 2009). Pyrazines possess unique and extremely potent flavor and aroma characteristics. Some of the derivatives of pyrazines find use as pharmaceutical intermediates, marking volatiles, antifungal and antiviral agents. Alkyl-substituted pyrazine is widely used as a key intermediate for pyrazineamide, an effective anti-tubercular drug (Prasad *et al*. 2013).

In pyrazine, pyridine and related six-membered heterocyclic molecules, resonance occurs as in benzene, causing the molecule to be planar and stable. In pyrazine, a large amount of intermolecular association is possible because of its greater polarity. The nitrogen lone pair is located in a SP^2 hybridized orbital which is perpendicular to π-system of the ring. A consequence

N. Prabavathi Tel. No.:+919791847378
E–mail: n.prabavathi@yahoo.co.in

of this structural feature is that the lone pair of electron on nitrogen atom is not associated with the ring and is available for protonation (Krishnakumar and Prabavathi, 2009).

Hence, the spectroscopic investigation of 3-amino-2-pyrazine carboxylicacid (APC) and methyl-3-amino-2-pyrazine carboxylate (MAPC) have been carried out and will be helpful in understanding various structural and spectral characteristics of these compounds.

2. EXPERIMENTAL DETAILS

The fine polycrystalline sample of APC and MAPC were obtained from Lancaster chemical company, UK, and used as such for the spectral measurements. The room temperature FTIR spectrum of the compounds were measured in the region 4000–400 cm^{-1} at a resolution of ±1cm^{-1}, using a BRUKER IFS-66V vacuum Fourier transform spectrometer equipped with a mercuryc admium telluride (MCT) detector, a KBr beam splitter and globar source. The FT-Raman spectrum was recorded on a BRUKER IFS–66V model interferometer equipped with an FRA–106 FT-Raman accessory. The spectrum was recorded in the 4000–50 cm^{-1} Stokes region using the 1064 nm line of a Nd :YAG laser for the excitation operating at 200mW power. The reported wave numbers are expected to be accurate within to ±1 cm^{-1}.

^{1}H and ^{13}C nuclear magnetic resonance (NMR) (400 MHz; CDCl3) spectra were recorded on a Bruker HC400 instrument. Chemical shifts for protons are reported in parts per million scale (d scale) downfield from tetramethylsilane.

The ultraviolet absorption spectra, in the region 200–1100 nm were recorded on a Lambda 35 spectrophotometer in 1.00 cm cells at 25 ± 0.1 °C. The spectra were run in spectra quality solvents (Fluka) using concentration of $5x10^{-5}$ M.

3. COMPUTATIONAL DETAILS

Calculations of structural parameters, vibrational frequencies, IR and Raman intensities of the chosen compounds have been carried out with Gaussian 09W software package (Benito Reyes-Trejo *et al.* 2014), using the B3LYP functional (Prabavathi *et al.* 2013) combined with standard 6-311++G** basis set. The energy minima with respect to the nuclear coordinates were obtained by the simultaneous relaxation of all the geometric parameters using the gradient methods.

The frequencies calculated on the basis of quantum mechanical force fields usually differ appreciably from observed frequencies. This was partly due to the neglect of anharmonicity and partly due to the approximate nature of the quantum mechanical methods (Prabavathi *et al.* 2013). In order to reproduce the observed frequencies, refinement of scaling factors were applied using the Molvib-7.0 program and optimized via least square refinement algorithm which resulted in a weighted RMS deviation between the experimental and scaled frequencies.

Root mean square (RMS) value was obtained using the following expression:

$$RMS = \sqrt{\frac{1}{n-1}\sum_{i}^{n}\left(\upsilon_i^{calcu} - \upsilon_i^{exp}\right)^2} \qquad (1)$$

The Raman activities (S_i) calculated by Gaussian program was suitably adjusted by the scaling procedure with Molvib and subsequently converted into relative Raman intensities (I_i) using the following relationship derived from the basic theory of Raman scattering.

$$I_i = \frac{f(\nu_0 - \nu_i)^4 S_i}{\nu_i[1-\exp(-hc\nu_i / kT)} \qquad (2)$$

where ν_0 is the exciting frequency (in cm^{-1} units), ν_i is the vibrational wave number of the i^{th} normal mode, h, c and k are fundamental constants and f is a suitably chosen common normalization factor for all peak intensities.

The first hyperpolarizability (β_0) and related properties (β, α_0 and $\Delta\alpha$) were calculated based on the finite-field approach. The theoretical calculation of β component is very useful to describe the direction of charge delocalization. This hyperpolarizability value also measures the non-linear optical activity of the molecular system.

The hyperpolarizability components (β_x, β_y, β_z) and the mean first hyperpolarizability (β_0) were calculated using the following expressions

$$\beta_0 = \left(\beta_x^2 + \beta_y^2 + \beta_z^2\right)^{1/2} \quad \text{and}$$

$$\beta_x = \beta_{xxx} + \beta_{xyy} + \beta_{xzz}$$

$$\beta_y = \beta_{yyy} + \beta_{xxy} + \beta_{yzz}$$

$$\beta_z = \beta_{zzz} + \beta_{xxz} + \beta_{yyz}$$

^1H and ^{13}C nuclear magnetic resonance chemical shifts of the molecules were also calculated using the gauge independent atomic orbital (GIAO) method. The theoretical UV–VIS spectrum of the compounds and the electronic properties, such as HOMO and LUMO energies were performed by time dependent DFT (TD-DFT) approach.

The natural bonding orbital (NBO) calculations were performed using NBO 3.1 program as implemented in the Gaussian 09 package in order to understand various second-order interactions between the filled orbitals of one subsystem and vacant orbitals of another subsystem, which is a measure of the intermolecular delocalization or hyper conjugation (Sebastian and Sundaraganesan, 2010).

4. RESULTS & DISCUSSION

4.1 Molecular Geometry

In order to find the most optimized geometry, the energy calculations for APC and MAPC were carried out for the possible conformers. The molecular geometry optimization was carried out for the conformer obtained with minimum energy. The optimized molecular structure of these compounds is shown in Fig. 1 along with atom numbering. The optimized molecular parameters of APC and MAPC are presented in Table 1. The molecular structure of these compounds belongs to C_s point group symmetry. From the structural data, it can be predicted that the amino group is planar with the pyrazine ring in both the molecules. All the dihedral angles on the benzene ring are either 0° or 180° and this indicate the planarity of the atoms and functional groups attached to the ring. The presence of functional group at the position C2 affects the regular hexagonal structure. The global minimum energy, zero-point vibrational energies, rotational constants, entropies and dipole moments obtained are presented in Table 2.

4.2 Spectral Analysis

The 39 and 48 modes of fundamental vibrations of these compounds are found to be distributed among the symmetry species as

For APC,

$$T_{3N-6} = 27\,A'\,(\text{in-plane}) + 12\,A''\,(\text{out-of-plane})$$

For MAPC,

$$T_{3N-6} = 33\,A'\,(\text{in-plane}) + 15\,A''\,(\text{out-of-plane})$$

The vibrational frequency assignments were made with the high degree of accuracy with the help of symmetry consideration, observed frequencies and PED obtained from the normal coordinate analysis. The unscaled, SQM frequencies, IR intensities and Raman scattering activities, potential energy distributions (PED) and assignment of the fundamentals for the title

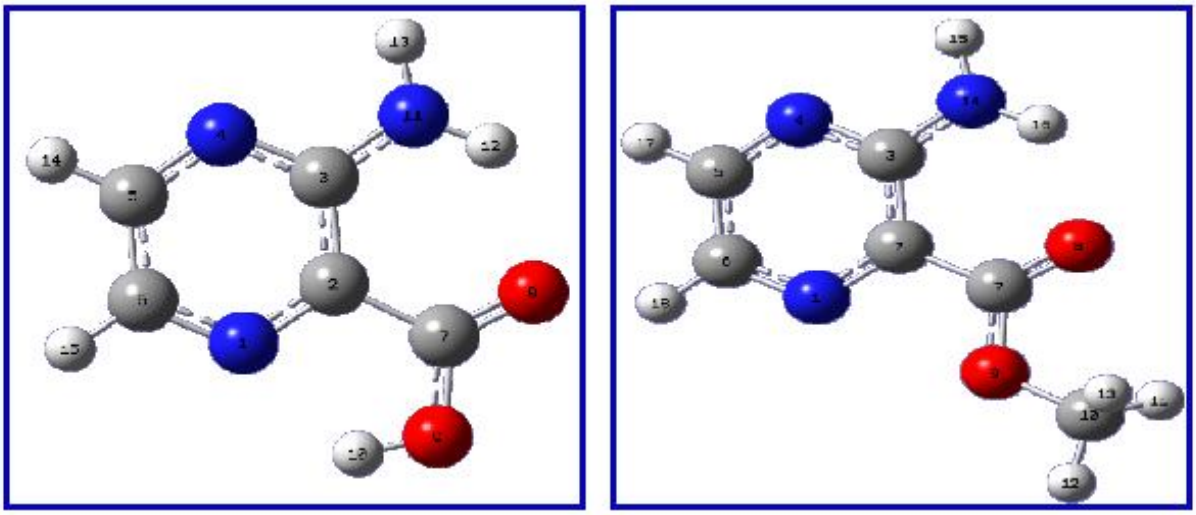

Fig. 1: Optimized geometries of APC and MAPC.

Table 1. Optimized geometrical parameters of APC and MAPC.

Parameters	Bond Length (Å)		Parameters	Bond angle (°)		Parameters	Torsional angle (°)	
	APC	MAPC		APC	MAPC		APC	MAPC
N1-C2	1.33	1.33	N1-C2-C3	121.11	120.90	N1-C2-C3-N4	0.0	0.0
C2-C3	1.43	1.43	C2-C3-N4	119.68	119.93	C2-C3-N4-C5	0.0	0.0
C3-N4	1.35	1.35	C3-N4-C5	117.57	117.48	C3-N4-C5-C6	0.0	0.0
N4-C5	1.32	1.32	N4-C5-C6	122.94	122.59	N4-C3-C2-C7	180.0	180.0
C5-C6	1.40	1.40	C3-C2-C7	122.66	120.59	N1-C2-C7-O8	180.0	180.0
C2-C7	1.49	1.49	C2-C7-O8	123.47	123.52	N1-C2-C7-O9	0.0	0.0
C7-O8	1.21	1.22	C2-C7-O9	114.47	113.58	C2-C7-O9-H10 (C10)	0.0	180.0
C7-O9	1.34	1.33	C7-O9-H10 (C10)	106.82	115.98	C7-O9-C10-H11	-	-60.0
O9-H10(C10)	0.98	1.44	O9-C10-H11	-	110.41	C7-O9-C10-H12	-	180.0
C10-H11	-	1.09	O9-C10-H12	-	105.37	C7-O9-C10-H13	-	60.0
C10-H12	-	1.09	O9-C10-H13	-	110.41	N1-C2-C3-N11 (N14)	180.0	180.0
C10-H13	-	1.09	C2-C3-N11 (N14)	122.61	123.48	C2-C3-N11 (N14)-H13 (H15)	180.0	180.0
C3-N11(N14)	1.35	1.35	C3-N11 (N14)-H13 (H15)	118.46	117.98	C2-C3-N11 (N14)-H12 (H16)	0.0	0.0
N11(N14)-H13(H15)	1.01	1.01	C3-N11 (N14)-H12 (H16)	119.28	119.54	C3-N4-C5-H14 (H17)	180.0	180.0
N11(N14)-H12(H16)	1.01	1.01	N4-C5-H14 (H17)	116.61	116.66	N4-C5-C6-H15 (H18)	180.0	180.0
C5-H14(H17)	1.09	1.09	C5-C6-H15 (H18)	121.97	121.54	-	-	-
C6-H15(H18)	1.08	1.08	-	-	-	-	-	-

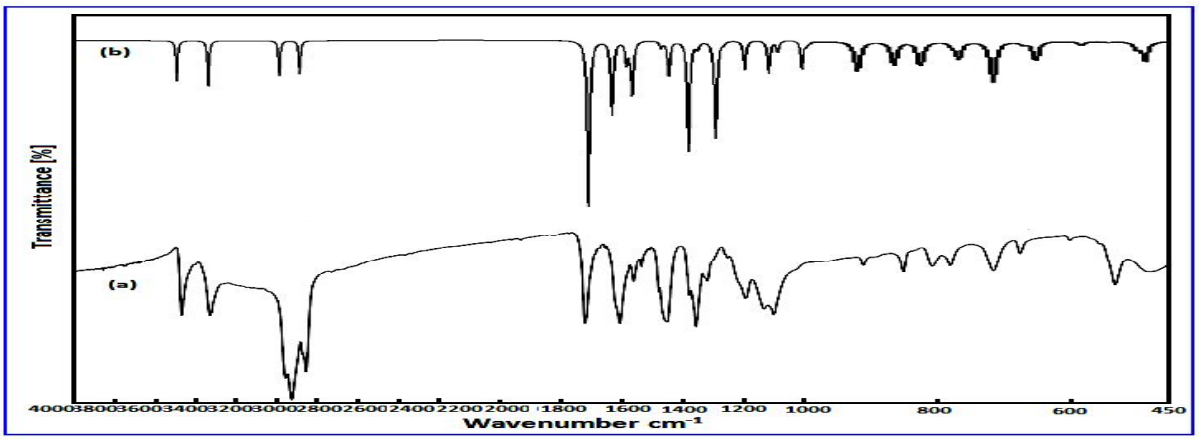

Fig. 2a: Comparison of observed and calculated FT-IR spectra of APC (a) observed and (b) calculated with B3LYP/6-311++G.**

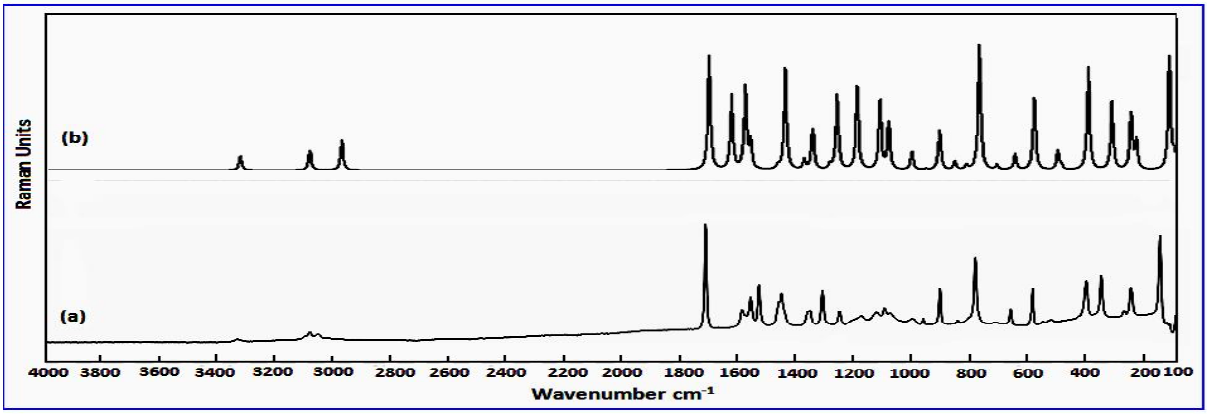

Fig. 2b: Comparison of observed and calculated FT-Raman spectra of APC (a) observed and (b) calculated with B3LYP/6-311++G.**

compounds are given in Table 3 and 4. For visual comparison, the observed and simulated FT-IR and FT-Raman spectra of these compounds are produced in common frequency scales in Figs. 2a-3b.

4.2.1 C-H Vibrations

The hetroaromatic structure shows the presence of C–H stretching vibrations in the region 3000–3100 cm^{-1}, which is the characteristic region for ready identification of C–H stretching vibrations (Krishnakumar and Prabavathi, 2009). In MAPC, the two stretching modes are predicted at 3193 and 3068 cm^{-1}. They are active in IR at 3193 cm^{-1} and Raman spectrum at 3068 cm^{-1}, respectively. The peak observed at 897 cm^{-1} in IR and 968 cm^{-1} in Raman is due to out-of-plane bending vibrations. The in-plane bending vibrations are established in IR at 1313 cm^{-1} and in Raman at 1251 cm^{-1}.

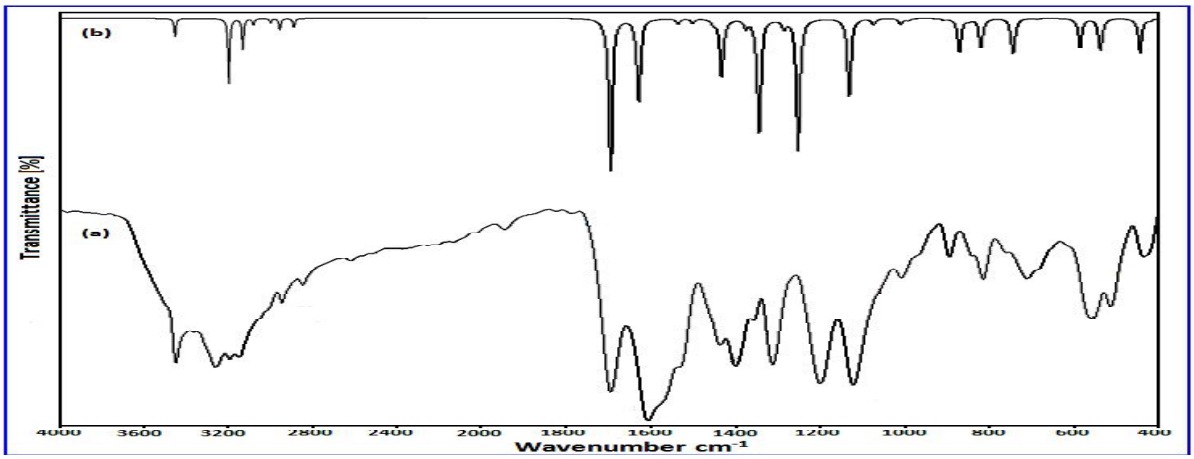

Fig. 3a: Comparison of observed and calculated FT-IR spectra of MAPC (a) observed and (b) calculated with B3LYP/6-311++G.**

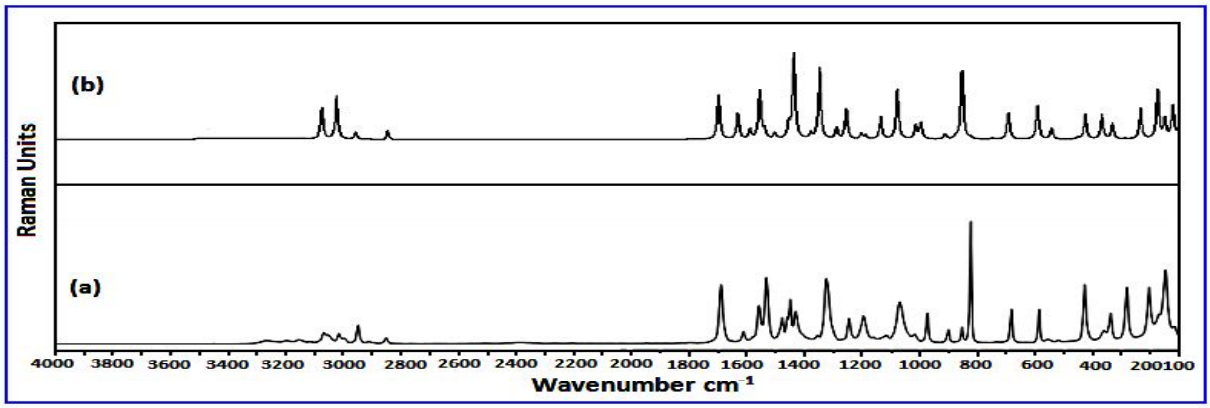

Fig. 3b: Comparison of observed and calculated FT-Raman spectra of MAPC (a) observed and (b) calculated with B3LYP/6-311++G.**

The APC stretching mode is observed at 2975 and 2875 cm^{-1} in the IR spectrum. The in-plane and out-of-plane bending modes are observed in the Raman spectrum at 1268, 1190 cm^{-1} and 968, 849 cm^{-1} respectively. All the vibrational frequencies were found to be well within their characteristic region.

4.2.2 NH_2 Vibrations of APC and MAPC

The NH_2 group has two N–H stretching vibrations, such as symmetric and antisymmetric stretching modes. The NH_2 asymmetric stretching vibrations give rise to a strong band in the region 3390 ± 60 cm^{-1} and the symmetric NH_2 stretching is observed as weak band in the region 3210 ± 60 cm^{-1} (Sebastian *et al*. 2013).

In APC and MAPC, the asymmetrical stretching vibrations are present in IR spectrum at 3480 and 3448 cm^{-1} respectively. The symmetric stretching vibration is observed somewhat at a lower region in the Raman spectrum at 3085 and 3017 cm^{-1} respectively.

Table 2. The calculated thermodynamic parameters of APC and MAPC.

Structural parameters	B3LYP/6- 311++G**	
	APC	MAPC
SCF energy (Hartrees)	-508.419	-547.724
Total energy (thermal), E_{total} (kcal mol^{-1})	73.09	91.38
Heat capacity at const. volume, Cv ($calmol^{-1}K^{-1}$)	30.79	36.38
Entropy, S (cal $mol^{-1}K^{-1}$)	88.34	98.38
Vibrational energy , E_{vib}($kcalmol^{-1}$)	71.31	89.60
Zero-point vibrational energy, E_0 (kcal mol^{-1})	68.04	85.13
Rotational constants (GHz)		
A	2.34845	2.23315
B	1.28870	0.84540
C	0.83209	0.61561
Dipole moment (Debye)		
μ_x	2.8883	-0.0577
μ_y	-2.4329	-0.2038
μ_z	0.0000	0.0000
μ_{total}	3.7764	0.2118

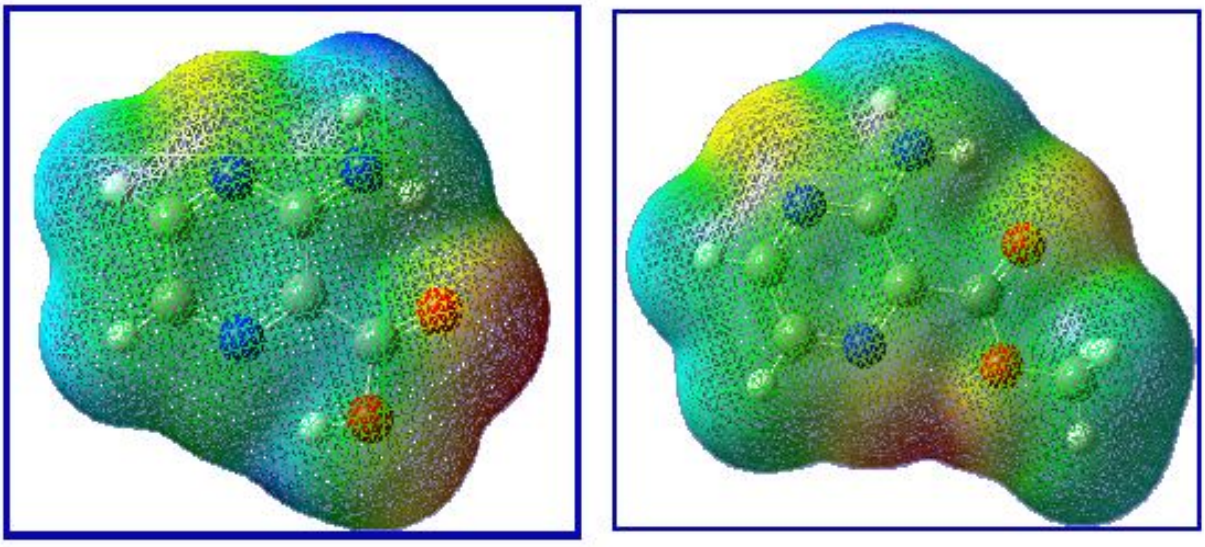

Fig. 4: The total electron density isosurface mapped with molecular electrostatic potential of APC and MAPC.

This may be due to the conjugation with ring π system. NH_2 scissoring vibrations give rise to a band in the region 1620 ± 20 cm^{-1} and rocking vibration in the range 1195 ± 90 cm^{-1} (Sebastian *et al.* 2013). In our study, the frequency observed at 1548 (APC) and 1608 cm^{-1} (MAPC) in IR spectrum were due to scissoring vibrations. The rocking modes of APC and MAPC are active in Raman spectrum at 1005 and 1068 $cm^{-1.}$ The calculated values for NH_2 scissoring and rocking modes are found to be at 1582 cm^{-1} (APC), 1585 cm^{-1} (MAPC) and 1007 cm^{-1} (APC), 1074 cm^{-1} (MAPC) respectively. The wagging and twisting vibrations occur usually as a multiple absorption bands in the region 909–666 cm^{-1} (Prabavathi *et al*. 2013). The twisting vibration is predicted at 670 and 682 cm^{-1} for APC and MAPC respectively.

4.2.3 Carboxylate vibrations of MAPC

The methyl vibrational band positions are most consistent when this group is attached to other carbon atoms. When the CH_3 group is directly attached to an oxygen atom, the C–H stretching and bending bands can shift position due to electronic effects. This causes the O–CH_3 stretching bands to be spread over a larger region than that of the C–CH_3 group (Lynnette Joseph *et al.* 2012). The two asymmetric stretching modes were observed in IR spectrum at 3260 and 3149 cm^{-1}, while the symmetric vibration establishes a peak in both IR and Raman spectra at 2945 and 2951 cm^{-1}.

The asymmetric bending vibrations of O-CH_3 groups normally appear in the region 1460 cm^{-1} (Lynnette Joseph *et al.* 2012). In MAPC, the two asymmetric bending vibrations are observed in Raman spectrum at 1534 and 1451 cm^{-1}. The symmetric bending vibration establishes a peak in IR spectrum at 1401 cm^{-1}. The rocking and torsional vibrations were also produced within their characteristic region.

The two C-O stretching vibrations computed at 1132 and 909 cm^{-1} corresponds to the peaks in Raman spectrum at 1117and 900cm^{-1}. The IR and Raman band observed at 1695 and 1685 cm^{-1}were assigned to the other C=O stretching mode of MAPC. Its predicted value is found to be 1693 cm^{-1} with 66% PED contribution.

4.2.4 COOH vibrations of APC

In very dilute solutions, the absorption caused by O-H stretching is observed near 3570 cm^{-1}. This broad band also appears for the acids which do not exist as dimers, in that, the negative charge on the O atom of OH reduces the bond order in OH due to the resonance (Mukherjee *et al.* 2011). In the present study the band at 3325 in IR is assigned to O-H stretching vibration and its corresponding calculated value is 3325 cm^{-1} with 100% PED contribution. The C=O stretching bands of acids are considerably more intense than ketonic C=O stretching bands. The characteristic infrared absorption frequency of C=O in acids are normally strong in intensity and found in the region 1800–1690 cm^{-1} (Prabavathi *et al.* 2012). For the titled compound, the band due to C-O stretching vibration is observed at 1710 and 1718 cm^{-1} in IR and Raman spectra respectively. The corresponding theoretically computed value is in good agreement with the experimental result with maximum PED contribution of 63%.

Two bands arising from C-O stretching and O-H bending appear in the spectra of carboxylic acid near 1210–1320 and 1400–1440 cm^{-1}, respectively. Both these bands involve some interaction between C-O stretching and in-plane C-O-H bending (Prabavathi *et al.* 2012). These two peaks are identified at 1365 and 1130 cm^{-1} in Raman spectrum. Since the OH bending mode occurs at 1412 cm^{-1} with strong IR intensity for benzoic acid (Prabavathi *et al.* 2012), the former frequency is assigned to the OH in-plane bending mode which is also observed with strong IR intensity and the later one is assigned to the C-O stretching mode. These are in good agreement with thepredicted values.

4.2.5 C-C Vibrations

In APC, the C-C stretching bands are observed in IR spectrum at 1448, 1100 (1102 in Raman) and 914 cm^{-1} (905 in Raman) . Their corresponding calculated

Table 3. Observed and B3LYP / 6-311++G level calculated vibrational frequencies (in cm^{-1}) of APC.**

S.No.	Symmetry species	Observed frequency (cm^{-1})		Calculated frequency (cm^{-1}) with B3LYP / 6 - 311++G** force field				PED (%) among type of internal coordinates
		IR	Raman	Unscaled	Scaled	IR[a] (I_i)	Raman[b] (A_i)	
1.	A'	3480	-	3700	3480	115.93	0.590	NH2ASS(99)
2.	A'	3325	-	3598	3325	131.67	37.320	OH(100)
3.	A'	-	3085	3541	3085	0.025	40.39	NH2SS(98)
4.	A'	2975	-	3191	2975	100.36	57.243	CH(98)
5.	A'	2875	-	3157	2875	95.922	0.044	CH(98)
6.	A'	1710	1718	1788	1707	471.45	62.417	COD(63),CC(7),CN(7)
7.	A'	1602	1598	1638	1630	210.61	37.684	CN(58),bring(11),CC(11)
8.	A'	1548	1568	1586	1582	62.371	39.448	NH2SCIS(52),CC(18)
9.	A'	1530	1534	1575	1564	152.27	12.678	CN(41),CC(21),NH2SCI(17)
10.	A'	-	1463	1494	1470	20.004	1.458	CN(37),bCH(31),NH2SCI(18)
11.	A'	1448	-	1460	1444	99.077	41.074	CC(33),NH2SCI(26),CN(18)
12.	A'	-	1365	1404	1379	314.83	3.687	bCOH(23),CC(18),COS(17)
13.	A'	1348	-	1362	1350	20.694	14.619	CN(48),bCH(34),COS(5)
14.	A'	1315	1308	1300	1291	275.43	1.595	CN(50),CC(21),bCOH(18)
15.	A'	-	1268	1271	1265	6.121	24.251	bCH(40),CN(31),CC(10)
16.	A'	1196	1190	1220	1196	83.446	24.698	bCH(30),bCOH(18),CC (14)
17.	A'	1115	1130	1119	1117	91.406	18.359	COS(31),CC(29),bCH(20)
18.	A'	1100	1102	1103	1087	30.920	11.831	CC(29), COS(20), NH2RO(14)
19.	A'	-	1005	1030	1007	81.930	3.909	NH2RO(57),CN(29),CC(8)
20.	A"	-	968	975	957	0.283	0.192	gCH(88),tring(11)
21.	A'	914	905	925	912	87.745	7.751	CC(75),CN(16), bring1(6)
22.	A"	850	849	858	859	67.811	1.434	gCH(47),gCC(18),tCO(17)
23.	A'	810	800	806	820	70.357	0.782	bCN(37),gCH(20),gCC(18)
24.	A'	775	-	772	774	8.961	19.127	bCC(39),CN(16),bOCO(14)
25.	A'	-	-	740	764	50.01	0.129	bOC(61),tCO(24),gCN(8)
26.	A"	714	-	708	714	121.35	0.715	tOH(91),tCO(5)
27.	A"	-	-	666	670	7.852	0.081	NH2TW(93)
28.	A'	670	668	657	651	54.720	1.854	bOCO(51),bring(19),bOC(10)
29.	A'	600	600	596	585	11.603	7.375	bring(82),CN(6)
30.	A"	-	546	566	545	2.734	0.013	gCC(43),tring(35),tCO(11),
31.	A'	500	-	541	504	20.008	1.519	bOC(37),bCC(23),bCN(18),
32.	A'	-	514	455	491	55.584	0.300	bring(49),gCC(32),tCO(10)
33.	A'	-	403	413	399	1.152	6.002	bring(34),CC(31),bCN(11)
34.	A"	-	-	362	366	154.99	0.001	tNH2(71),NH2TW(14),tring(10)
35.	A"	-	368	322	317	1.484	2.792	gCN(72),bOC(12)
36.	A"	-	285	241	251	2.077	1.588	tring(48),gCC(22),tCO(19)
37.	A"	-	251	239	233	22.067	0.707	tring(52),bOC(33)
38.	A"	-	151	113	119	0.986	0.887	tCO(55),tring(24),NH2TW(10)
39.	A"	-	100	100	102	0.149	0.088	tring(82),NH2TW(9)

Abbreviations used: b-bending; g-deformation; ass-asymmetric; ss-symmetric; t-torsion; sci-scissoring.
[a] Relative absorption intensities normalized with highest peak absorption.
[b] Relative Raman intensities calculated and normalized to 100.

values are predicted at 1444, 1087 and 912 cm^{-1} respectively. For MAPC molecule, the calculated C-C stretching values are found at 1375, 1344 and 993 cm^{-1}. It has the experimental counterpart in IR spectrum at 1367, 1010 cm^{-1} and in Raman at 1334 cm^{-1}. The CCC in-plane and out of plane bending vibrations of these compounds were completely assigned and are presented in Table 3 and 4.

4.2.6 C-N Vibrations

The identification of C–N vibrations is a difficult task, since the mixing of vibrations is possible in this region. However, with the help of the force field calculations, the C–N vibrations are identified and assigned in this study. The bands appearing at Raman spectrum at 1617, 1017, 1568, 1485 and 1434 cm^{-1} are all assigned to C-N vibrations of MAPC. For APC, the four C-N vibrations are present in IR at 1602, 1530, 1348 and 1315 cm^{-1} and one is present in Raman only at 1463 cm^{-1}. The C-N in-plane and out of plane bending vibrations of the compounds are completely assigned and are presented in Table 3 and 4.

4.3 Hyperpolarizability

The first hyperpolarizability values are found to be $2.2636 * 10^{-30}$ e.s.u. (APC) and $1.7235* 10^{-30}$ e.s.u. (MAPC). The values of the hyperpolarizability (β) components are given in Table 5. The maximum charge delocalization is present along β_{xxx} and β_{xyy} for APC and MAPC respectively. The charge delocalization is absent for both the molecules along $\beta_{xxz,}$ $\beta_{xyz,}$ β_{yyz} and β_{zzz} direction.

4.4 Molecular Electrostatic Potential (MESP)

Molecular electrostatic potential (MESP) at a point in the space around a molecule gives an indication of the net electrostatic effect produced at that point by the total charge distribution (electron + nuclei) of the molecule and correlates with dipole moments, electro negativity, partial charges and chemical reactivity of the molecule. It provides a visual method to understand the relative polarity of the molecule. An electron density isosurface mapped with electrostatic potential surface depicts the size, shape, charge density and site of chemical reactivity of the molecule. The different values of the electrostatic potential represented by different colors; red represents the regions of the most negative electrostatic potential, blue represents the regions of the most positive electrostatic potential and green represents the region of zero potential. Potential increases in the order red < orange < yellow < green < blue (Kannan *et al*. 2012). The fig. 4 represent the molecular electrostatic potential surfaces of APC and MAPC molecules. In APC, the negative regions are mainly localized on the oxygen atoms and to some extent on the N4 atom. All the other atoms are considered to be an active nucleophilic site.In MAPC, the atoms O8, O9, N1 and N4 are considered to be an electrophilic site of the molecule.In both the molecules, green areas cover parts of the molecule where electrostatic potentials are close to zero (C-C bonds). The amino group hydrogens are blue in colour and give a positive potential that explains the delocalization towards the ring. Thus, this figure provides a visual representation of the chemically active sites and comparative reactivity of atoms.

4.5 NMR Analysis

NMR shielding contains detailed information about the electronic structure of molecules. The chemical shifts of carbon and hydrogen atoms of these compounds are studied experimentally and theoretically. The experimental and theoretical values for ^{1}H and ^{13}C NMR of APC and MAPC were given in Table 6. The experimentally and theoretically computed ^{13}C and ^{1}H NMR spectra of APC and MAPC are shown in figs. 5 - 8.

The carbon C3 situated between the ring nitrogen and an amino group experience a downfield in both the compounds. The C7 atom with oxygen on either side deshields it to a greater extent and gives a chemical shift of about 167 ppm. The C2, C5 and C6 atom observes nearly same chemical shift in both the compounds. The methoxy hydrogens experience a chemical shift by about

Table 4. Observed and B3LYP / 6-311++G level calculated vibrational frequencies (in cm^{-1}) of MAPC.**

S.No.	Symmetry species	Observed frequency (cm^{-1})		Calculated frequency (cm^{-1}) with B3LYP / 6 - 311++G** force field				PED (%) among type of internal coordinates
		IR	Raman	Unscaled	Scaled	IR[a] (I_i)	Raman[b] (A_i)	
1.	A'	3448	-	3704.4	3448.0	40.520	197.855	NH2ASS(99)
2.	A"	3260	-	3551.7	3260.0	19.510	55.949	OCH3ops(100)
3.	A'	3193	-	3174.5	3193.0	25.179	201.524	CH(99)
4.	A'	3149	-	3163.9	3149.0	9.394	68.773	OCH3ips(99)
5.	A'	-	3068	3147.9	3068.0	13.835	152.518	CH(99)
6.	A'	-	3017	3117.6	3017.0	69.940	207.755	NH2SS(84)
7.	A'	2945	2951	3049.6	2951.0	144.394	31.355	OCH3ss (83)
8.	A'	1695	1685	1722.5	1693.3	339.419	56.541	COD(66),COS(7),CC(5)
9.	A'	-	1617	1629.2	1627.0	183.697	29.322	CN(64),bring1(12),NH2SCI(9)
10.	A'	1608	-	1586.0	1584.6	0.839	10.751	NH2SCI(90),OCH3ip(8)
11.	A'	-	1568	1567.7	1551.2	0.538	52.520	CN(40),bCH(34),NH2SCI(9)
12.	A'	-	1534	1499.6	1534.1	11.818	9.590	OCH3ipb(88),OCH3op(11)
13.	A'	-	1485	1488.0	1499.7	10.037	5.737	CN(31),NH2SCI(24),CC(18)
14.	A"	-	1451	1480.0	1451.0	10.207	13.772	OCH3opb(60),CC(10),COS(9)
15.	A'	1437	1434	1471.3	1433.8	30.168	60.232	CN(43),bCH(35),NH2SCI(5)
16.	A'	1401	-	1448.5	1430.4	106.221	26.470	OCH3sb(19),COS(18),CC(17)
17.	A'	1367	-	1365.6	1374.9	19.706	4.581	CC(43),bCH(35),bCC(6)
18.	A'	-	1334	1340.1	1343.8	252.548	59.856	CC(58),CN(13),NH2RO(7)
19.	A'	1313	-	1270.1	1285.0	20.129	8.331	bCH(69),COS(12),bCOC(7)
20.	A'	-	1251	1244.8	1251.5	294.141	21.853	bCH(89),OCH3op(10)
21.	A'	1201	-	1211.8	1199.4	0.386	3.857	CH3ipr(38),bring1(17),CC(5)
22.	A'	-	1185	1169.9	1185.0	0.333	2.451	CH3opr(44),NH2RO(24),bCH(16)
23.	A'	-	1117	1138.4	1132.0	171.297	14.042	COS(30),NH2RO(29),CC(25)
24.	A'	-	1068	1102.4	1074.4	13.424	29.746	NH2RO(44),CC(24),bCH(16)
25.	A'	-	1017	1030.4	1010.6	13.051	7.513	CN(30),NH2RO(29),CC(25)
26.	A'	1010	-	985.0	993.1	4.876	8.112	CC(55),bring(19),CC(10)
27.	A"	-	968	976.1	986.9	0.232	0.159	gCH(89),tring(10)
28.	A'	-	900	911.0	909.3	3.647	2.318	COS(50),bCC(17),CN(12)
29.	A"	897	-	866.1	872.4	74.878	1.078	gCH(96)
30.	A'	-	851	829.9	850.1	3.844	27.882	bOCO(35),bCOC(14),COS(10)

31.	A'	816	817	823.3	821.7	64.122	0.729	bCN(40),gCN(19),tCOC(16)
32.	A'	-	-	750.3	746.4	78.974	0.356	bCOC(41),tCOC(37),gCN(10)
33.	A'	712	-	686.4	690.3	1.554	7.666	bring(40),CC(20),bCCO(15)
34.	A"	-	685	654.6	681.8	0.009	0.453	NH2TW(73),tring(10),tCOC(8)
35.	A'	-	585	592.1	589.0	65.640	8.348	bring(80),CN(7)
36.	A"	558	551	561.7	550.3	2.365	0.031	gCN(50),tring(29),gCH(8)
37.	A'	516	517	516.9	540.3	70.503	2.321	bCCO(28),bCN(22),bCC(11)
38.	A"	-	-	464.5	448.1	77.306	0.246	gCC(64),tring(21),tCOC(10)
39.	A'	437	434	412.0	423.2	3.844	3.634	bring(43),bCCO(20),CC(10)
40.	A'	-	368	349.3	365.5	17.071	2.923	bCC(51), tring(21),CC(10)
41.	A"	-	354	334.4	329.3	5.309	1.571	tring(30),bring(18),bCN(14)
42.	A"	-	285	299.1	285.9	181.449	0.041	tring(84),tNH2(11)
43.	A"	-	217	265.5	231.8	6.383	1.724	tNH2(30),gCC(29),tring(22)
44.	A"	-	168	174.1	172.4	2.465	1.741	tOCH3(62),bOCO(17),bCOC(12)
45.	A"	-	151	152.5	148.0	0.451	0.503	tOCO(51),tCOC(22),tring(16)
46.	A"	-	117	128.5	120.2	0.016	0.599	tring(33),NH2TW(16),tCOC(14)
47.	A"	-	-	85.3	76.5	8.829	1.158	tCOC(32),gCC(27),tring(21)
48.	A"	-	-	55.8	55.8	0.028	0.373	tOC(92)

Abbreviations used: b-bending; g-deformation; ass-asymmetric; ss-symmetric; t-torsion; sci-scissoring.
[a] Relative absorption intensities normalized with highest peak absorption.
[b] Relative Raman intensities calculated and normalized to 100.

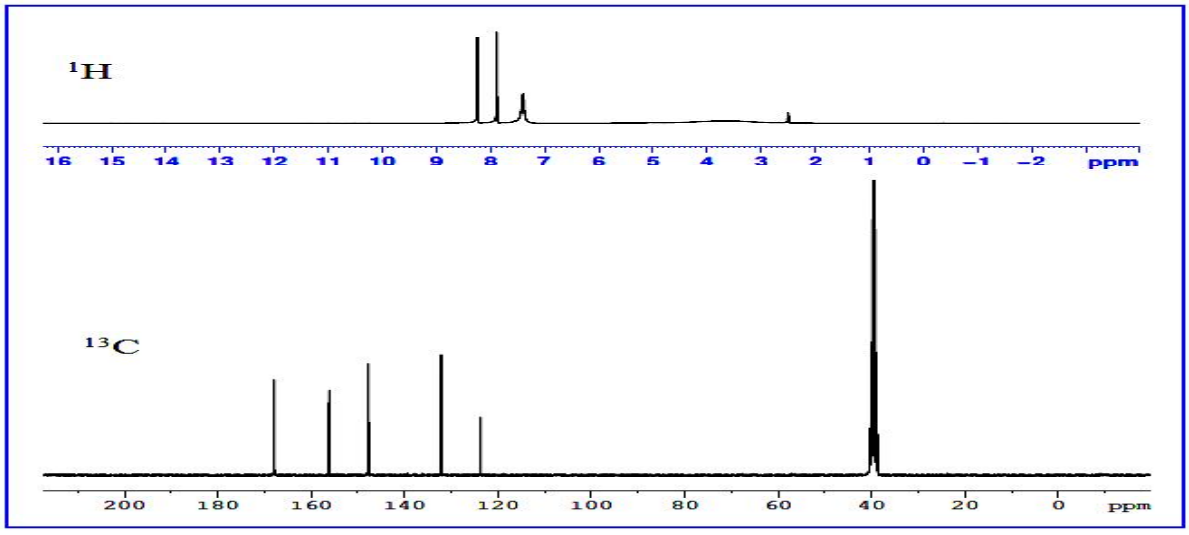

Fig. 5: Experimental NMR spectrum of ^{13}Cand ^{1}H of APC.

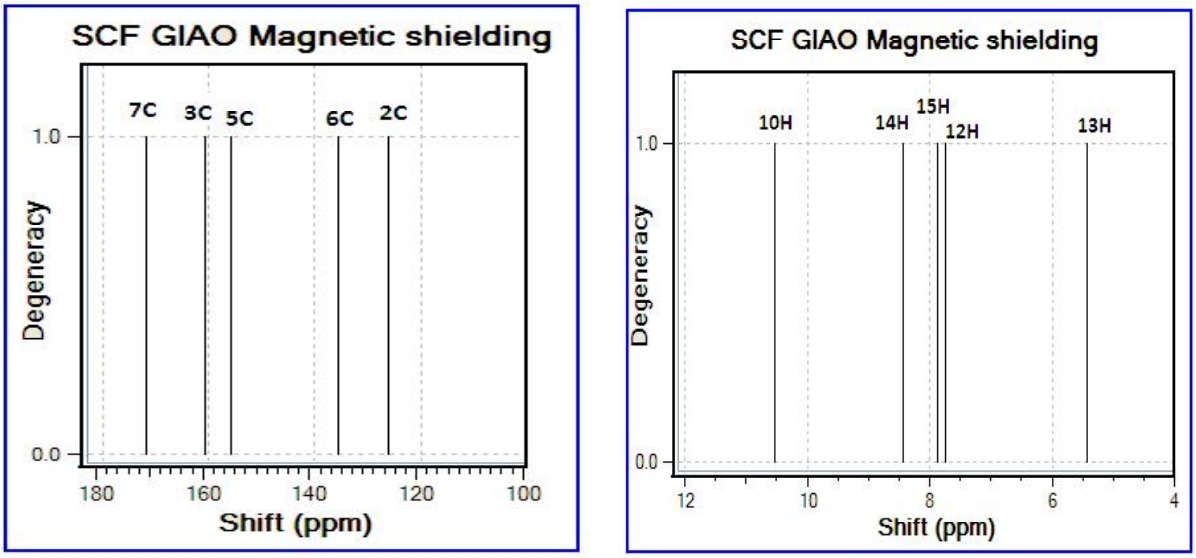

Fig. 6: Theoretical NMR spectrum of ^{13}Cand ^{1}H of APC.

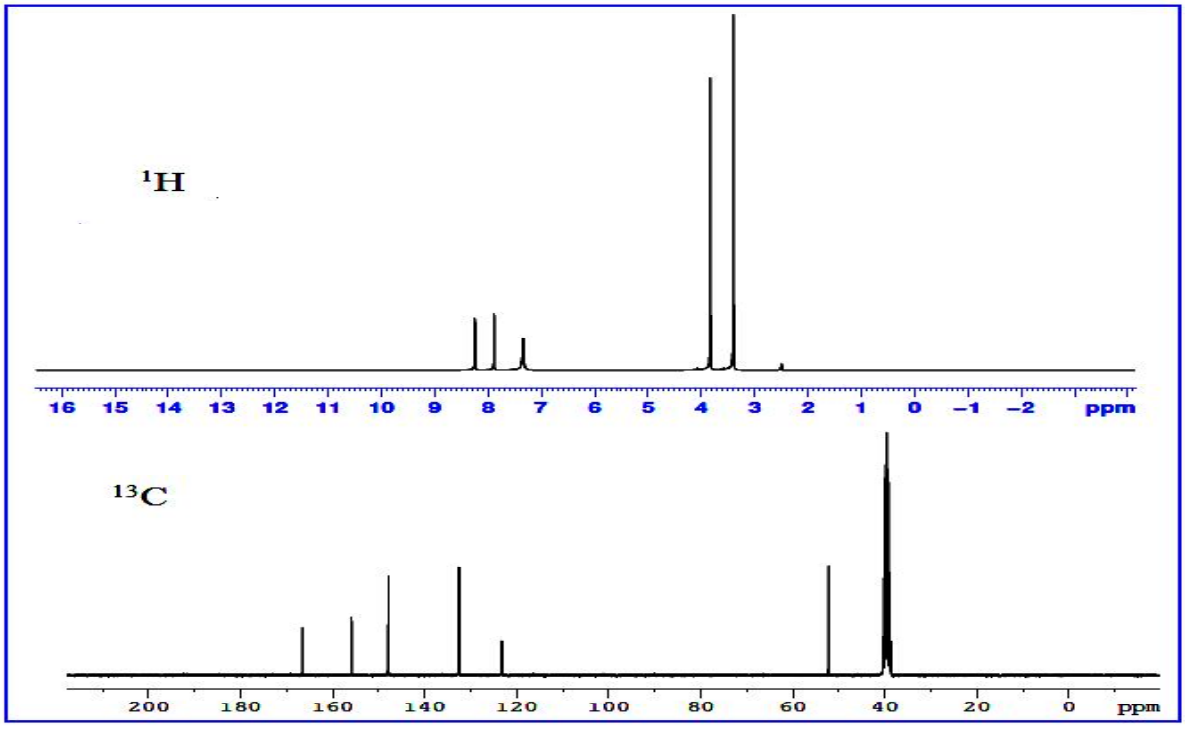

Fig. 7: Experimental NMR spectrum of ^{13}Cand ^{1}H of MAPC.

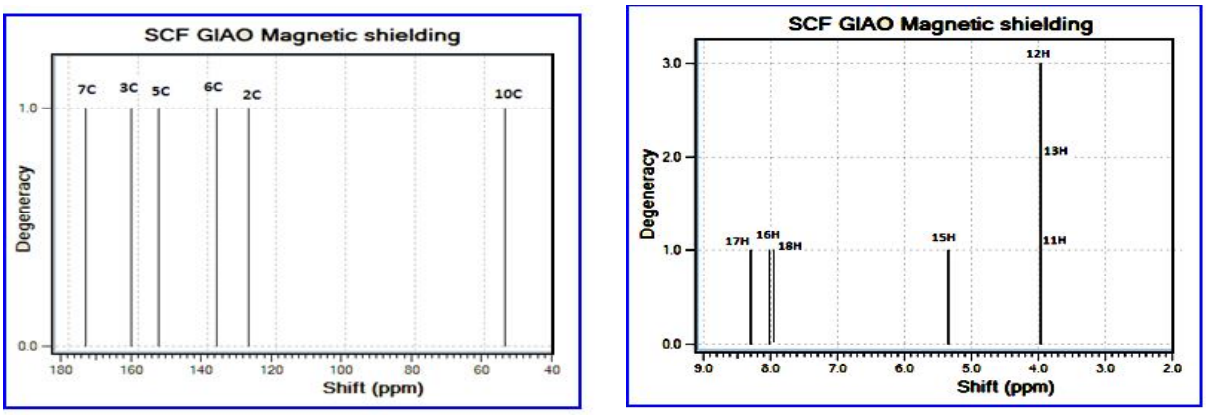

Fig. 8: Theoretical NMR spectrum of ^{13}C and ^{1}H of MAPC.

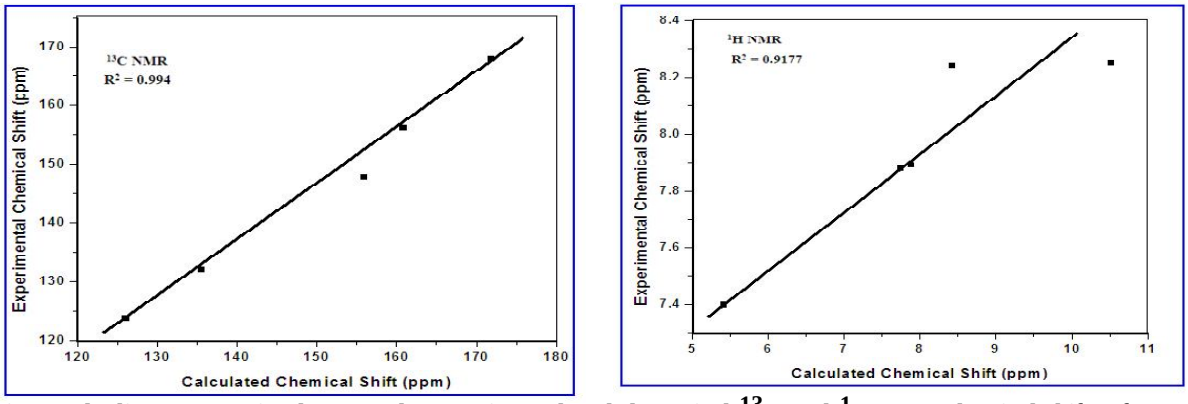

Fig. 9: The linear regression between the experimental and theoretical ^{13}C and ^{1}H NMR chemical shifts of APC.

Table 5. Calculated all β components and β_{tot} value of APC and MAPC

β - Component	B3LYP/6-311++G(d,p)	
	APC	MAPC
β_{xxx}	320.666	-50.501
β_{xxy}	109.402	-48.916
β_{xyy}	-116.947	255.676
β_{yyy}	31.013	106.257
β_{xxz}	0.0	0.0
β_{xyz}	0.0	0.0
β_{yyz}	0.0	0.0
β_{xzz}	29.605	-16.133
β_{yzz}	-21.185	6.399
β_{zzz}	0.0	0.0
$\beta_{total(esu)}$	2.2636×10^{-30}	1.7235×10^{-30}

Table 6. The experimental and calculated ^{1}H and ^{13}C isotropic chemical shift (with respect to TMS, all values in ppm) for APC and MAPC.

APC			MAPC		
Atoms	Experimental	Theoretical	Atoms	Experimental	Theoretical
C_2	123.76	126.05	C2	123.23	128.11
C_3	156.16	160.85	C3	155.92	162.02
C_5	147.78	155.88	C5	147.87	154.08
C_6	132.13	135.51	C6	132.54	137.12
C_7	167.95	171.86	C7	166.51	174.92
H_{10}	8.25	10.52	C10	52.16	53.91
H_{12}	7.88	7.75	H11	3.4	3.97
H_{13}	7.40	5.42	H12	3.4	3.97
H_{14}	8.24	8.43	H13	3.4	3.97
H_{15}	7.89	7.88	H15	3.83	5.35
-	-	-	H16	7.89	8.02
-	-	-	H17	8.26	8.29
-	-	-	H18	7.3	7.95

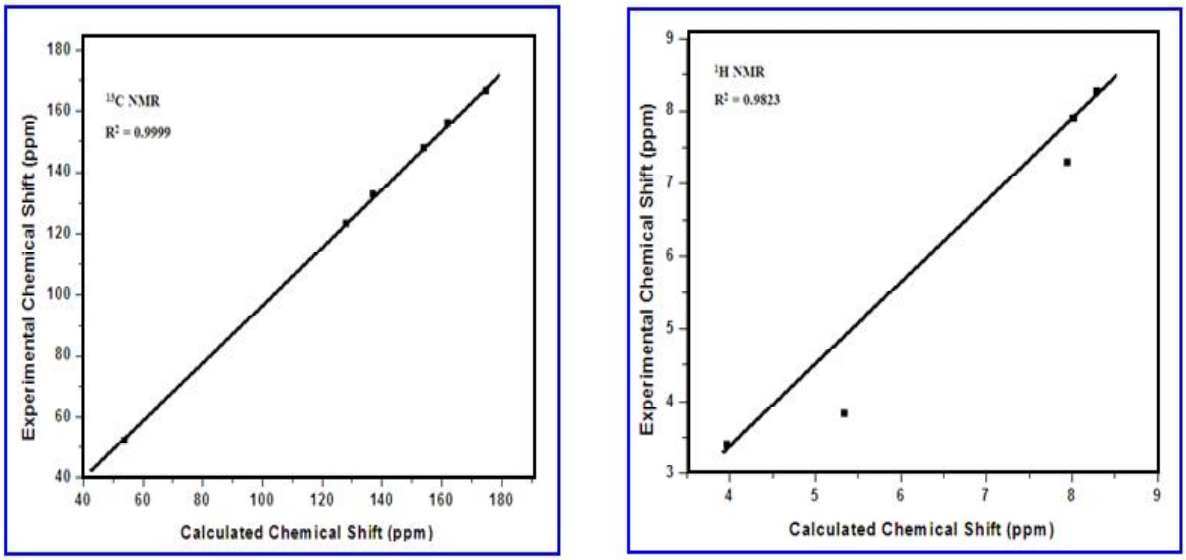

Fig. 10: The linear regression between the experimental and theoretical ^{13}C and ^{1}H NMR chemical shifts of MAPC.

Table 7. Experimental and theoretical electronic absorption spectra values of APC and MAPC.

Excited state	Wavelength λ (nm)				Excitation energies (eV)		Oscillator strengths (f)	
	Experimental		Theoretical					
	APC	MAPC	APC	MAPC	APC	MAPC	APC	MAPC
S1	240.89	284.8	254.69	332.43	4.8681	3.7296	0.0004	0.1785
S3	-	229.3	316.33	236.62	3.9195	5.2398	0.0031	0.1953
S2	345.02	205.40	333.50	210.83	3.7176	5.8807	0.1509	0.0126

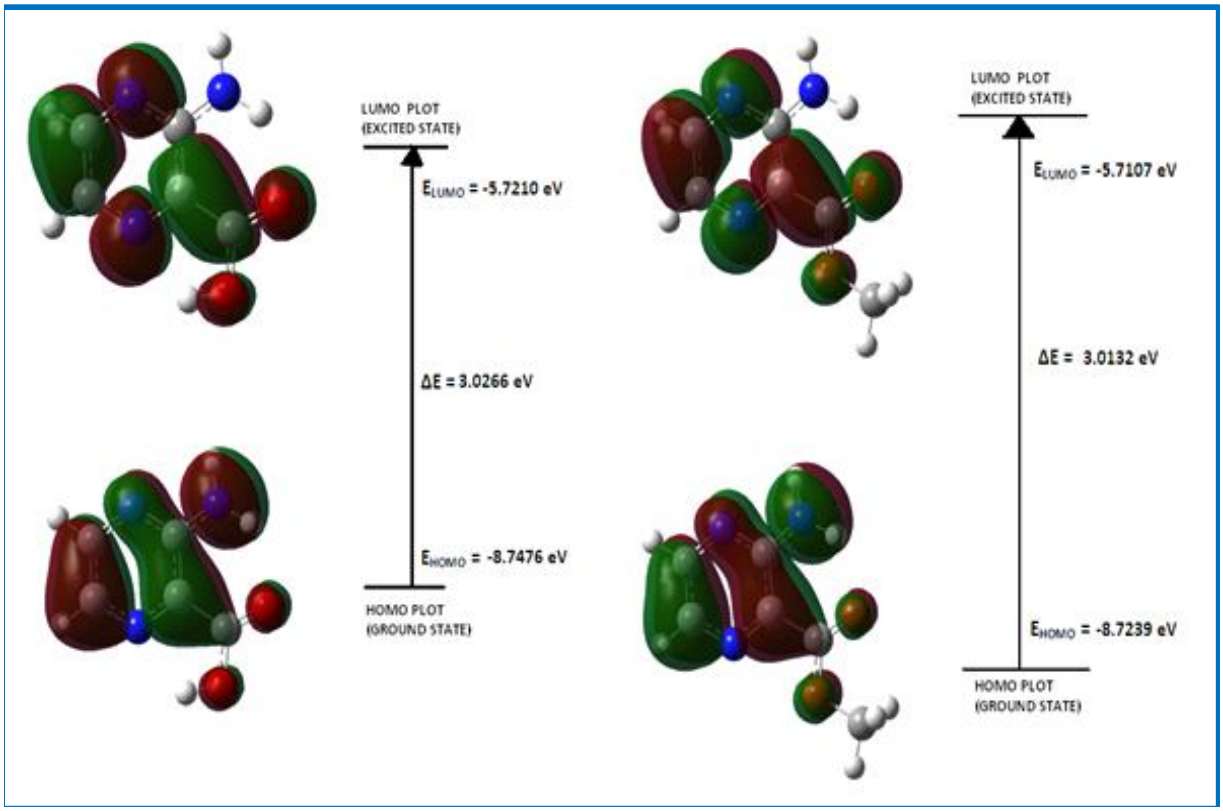

Fig. 11: The atomic orbital compositions of the frontier molecular orbital for APC and MAPC.

3.4 ppm. The C5 and C6 attached hydrogens observes a downfield by about 8.2 and 7.5 ppm. The linear regression curves show a good agreement between the experimental and theoretical chemical shifts and are given in figs. 9 and 10.

4.6 Frontier Molecular Orbitals

The HOMO–LUMO orbitals computed at B3LYP/6-311++G**level for the titled compounds are illustrated in fig 11. In APC and MAPC, at homo level the delocalization has been occurred on all the atoms except in –CH3 group of MAPC. At lumo level, the delocalization is absent in the amino group of both the compounds. The predicted energy gap value reflects the chemical reactivity of the molecule.

4.7 UV-Vis Analysis

The time-dependent density functional theory (TD-DFT) calcu-lation has been performed.The experimentally and theoretically predicted UV–Vis spectra are visualized in fig. 12 and 13. The λ_{max} values are obtained from the UV-Vis spectrum and compared with the theoretical values. The absorption maxima which are a function of electron availability, theoretical electronic excitation energies and oscilla-tor strength are given in Table 7. In APC and MAPC, the $\pi \rightarrow \pi^*$

Table 8. Mulliken atomic charges for optimized geometry of APC and MAPC

APC		MAPC	
Atom	Mulliken charges	Atom	Mulliken charges
N1	-0.084	N1	-0.077
C2	0.125	C2	0.655
C3	0.055	C3	-0.181
N4	-0.151	N4	-0.126
C5	-0.171	C5	-0.174
C6	0.059	C6	0.193
C7	-0.276	C7	-0.836
O8	-0.344	O8	-0.299
O9	-0.166	O9	-0.085
H10	0.288	C10	-0.212
N11	-0.355	H11	0.184
H12	0.321	H12	0.160
H13	0.299	H13	0.184
H14	0.198	N14	-0.398
H15	0.202	H15	0.289
-	-	H16	0.324
-	-	H17	0.196
-	-	H18	0.204

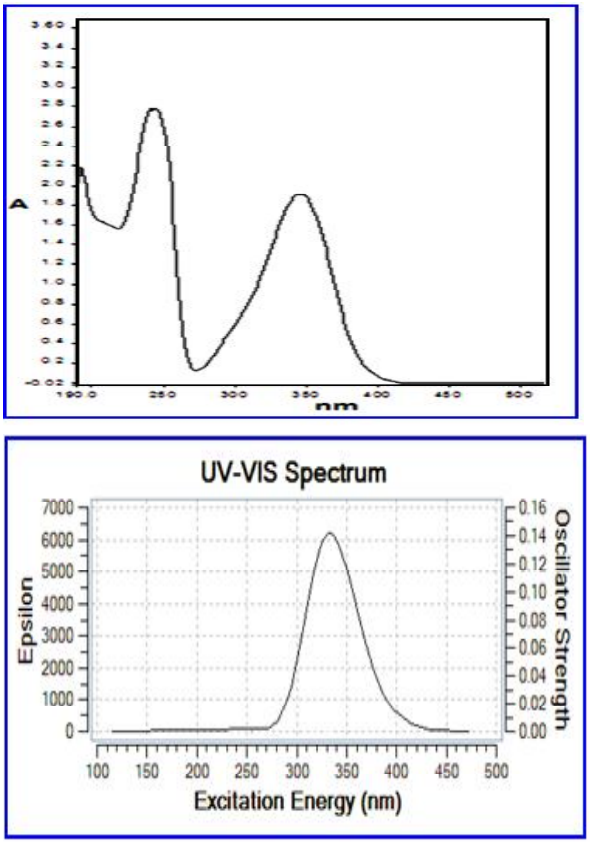

Fig. 12: Experimental and Theoretical UV-Vis spectrum of APC.

Table 9. The Second-order perturbation energies E(2) (Kcal/mol) corresponding to the most important charge transfer interactions (donor-acceptor) in APC and MAPC by B3LYP/6-311++G method.**

NBO(i)	Type	ED/e	NBO(j)	Type	ED/e	E (2)[a] (kJ mol^{-1})	E (j)–E(i) b (a.u.)	F (i, j) c (a.u.)	ED_A(%) (a.u) of j	ED_B (%) (a.u) of j
APC										
N1 – C6	Π	1.74206	N4-C5	π*	0.34477	19.69	0.31	0.072	38.98	61.02
C2-C7	Σ	1.98093	N1-C6	σ*	0.01620	3.94	1.22	0.062	39.60	60.40
N4-C5	Π	1.75496	N1-C6	π*	0.40522	13.67	0.30	0.060	45.00	55.00
N1	LP(1)	1.90550	C2-C3	σ*	0.04687	9.35	0.87	0.082	50.01	49.99
			C2-C7	σ*	0.07920	4.02	0.78	0.050	47.69	52.32
			C5-C6	σ*	0.03249	7.65	0.91	0.076	49.90	50.10
			C6-H15	σ*	0.02133	3.68	0.79	0.049	39.64	60.36
			O9-H10	σ*	0.02396	5.57	0.78	0.060	24.10	75.90
C2	LP(1)	1.06151	N1-C6	π*	0.40522	87.26	0.13	0.109	45.00	55.00
			C7-O8	π*	0.27163	55.28	0.15	0.099	70.49	29.51
O8	LP(2)	1.85421	C2-C7	σ*	0.07920	16.78	0.67	0.097	47.68	52.32
			C7-O9	σ*	0.08220	29.84	0.65	0.126	67.18	32.82
			N11-H12	σ*	0.01773	4.31	0.71	0.051	27.77	72.23
O9	LP(2)	1.80483	C7-O8	π*	0.27163	48.83	0.33	0.116	70.49	29.51
MAPC										
N1-C6	Π	1.72796	N4-C5	π*	0.34798	21.47	0.30	0.074	38.75	61.25
N4-C5	Π	1.75945	N1-C6	π*	0.37298	12.95	0.31	0.059	46.97	53.03
C2	LP(1)	1.07632	N1-C6	π*	0.37298	81.53	0.13	0.110	46.97	53.03
			C7-O8	π*	0.29650	65.84	0.13	0.101	71.64	28.36
O8	LP(2)	1.85817	C2-C7	σ*	0.06931	15.74	0.69	0.095	48.64	51.36
			C7-O9	σ*	0.08664	29.32	0.66	0.126	68.16	31.84
O9	LP(2)	1.77756	C7-O8	π*	0.29650	51.06	0.32	0.117	71.64	28.36
			C10-H11	σ*	0.01330	4.54	0.72	0.054	40.36	59.64
			C10-H13	σ*	0.01330	4.54	0.72	0.054	40.36	59.64

[a] E (2) means energy of hyper conjugative interaction (stabilization energy);
[b] Energy difference between donor and acceptor i and j NBO orbitals;
[c] F (i, j) is the Fock matrix element between i and j NBO orbitals.

transition are observed at 240.89, 345.02 and 284.8, 229.3, 205.40 nm. All these absorption maxima are predicted theoretically with excitation energy more than 3.5 eV.

4.8 Mulliken Atomic Charges

The Mulliken atomic charges are collected in Table 8. The amino group nitrogen and hydrogen found to possess higher magnitude of charge in both the compounds. The C10 atom in MAPC attracts the electrons from O9 and neutralizes it and the C7 atom present between O8 and O9 atom has a higher negative charge.

4.9 NBO Analysis

The NBO analysis was carried out to assess the most significantly interacting NBOs with their

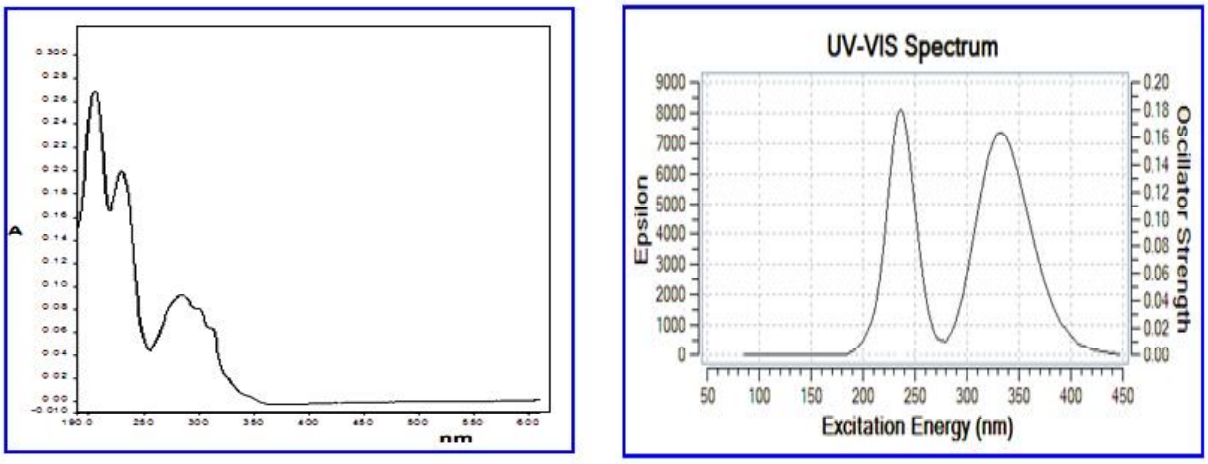

Fig. 13: Experimental and Theoretical UV-Vis spectrum of MAPC

constituent hybrids. The polarization coefficients, occupancies, hybrid composition of NAO's and their second order perturbation stabilization energies E(2) have been shown in the Table 9.

For APC, an important hyperconjugative interaction have been predicted for the charge transfer between LP(1)C2 →π*(N1-C6), LP(1)C2 →π*(C7-O8) and LP(2)O9→ π*(C7-O8) resulting with a stabilization energy of about 87.26, 55.28 and 48.83 respectively. The interaction from LP(1)N1 to σ*(C2-C3), σ*(C2-C7), σ*(C5-C6), σ*(C6-H15) and σ*(O9-H10) produces a stabilization energy of about 9.35, 4.02, 7.65, 3.68 and 5.57 kJmol^{-1} respectively. The LP(2)O8 to σ*(C2-C7), σ*(C7-O9), σ*(N11-H12) gives a stabilized energy of about 16.78, 29.84 and 4.31 kJmol^{-1} respectively. The π electron delocalization from N1-C6 and N4-C5 distributed to π* of N4-C5 and N1-C6 produces a stabilization energy of about 19.69 and 13.67 kJmol^{-1}, respectively.

In MAPC, LP(1)C2 → π*(N1-C6), LP(1)C2 → π*(C7-O8), LP(2)O9 → π(C7-O8) gives a higher stabilization energy of about 81.53, 65.84 and 51.06 kJmol^{-1}, respectively. The other interaction producing appreciably higher energies are given in Table 9.

5. CONCLUSION

The FT-IR and FT-Raman spectral data shows good correlation with the theoretically computed values. The computed ^{13}C and ^{1}H NMR chemical shift are in good agreement with the experimental values. Both the molecules are highly reactive and can be used for many applications. All the absorption maxima (λ_{max}) are due to π → π* transitions. The Mulliken charge analysis provides a proper understanding of the atomic theory. The NBO analysis clearly demonstrates the hyper conjugative interactions that occur within the molecule.

ACKNOWLEDGEMENT

The financial support from the University Grants Commission under Major Research Project scheme [F. No. 39-454/2010(SR)] is acknowledged. We are also pleased to recognize the generous support

given by St. Joseph's College, Trichy in recording the uv-vis spectrum.

REFERENCES

Benito Reyes-Trejo, Diana Guerra-Ramirez, Holber Zuleta-Prada, Rosa Santillan, Maria Elena Sanchez-Mendoza, Jesus Arrieta and Lino Reyes, Molecular Disorder in (-)-Encecanescin, *Molecules*, 19, 4695-4707(2014)
doi:10.3390/molecules19044695

Chacko YohannanPanicker, HemaTresa Varghese and ThahaThansani, Spectroscopic studies and Hartree-Fockab initio calculations of a substituted amide of pyrazine-2-carboxylic acid-$C_{16}H_{18}ClN_3O$, *Turk J Chem.*, 33, 633–646(2009).
doi:10.3906/kim-0808-14

Karnan, M., Balachandran, V. and Murugan, M., Vibrational spectroscopic (FT-IR and FT-Raman) studies, natural bond orbital analysis and molecular electrostatic potential surface of 3-hydroxy-6-methyl-2-nitropyridine, *Spectrochim. Acta Part A.*, 96, 51–62(2012).
doi:10.1016/j.saa.2012.05.007

Krishnakumar, V. and Prabavathi, N., Scaled quantum chemical calculations and FTIR, FT-Raman spectral analysis of 2-Methylpyrazine, *Spectrochim.Acta Part A.*, 72, 743–747(2009).
doi:10.1016/j.saa.2008.11.012

Lynnette Joseph, Sajan, D., Reshmy, R., ArunSasi, B. S., Erdogdu, Y. and Kurien Thomas, K., Vibrational spectra, structural conformations, scaled quantum chemical calculations and NBO analysis of 3-acetyl-7-methoxycoumarin, *Spectrochim. Acta Part A.*,99, 234–247(2012).
doi:10.1016/j.saa.2012.07.084

Mukherjee, V., Singh, N. P. and Yadav, R. A., Optimized geometry and vibrational spectra and NBO analysis of solid state 2,4,6-tri-fluorobenzoic acid hydrogen bonded dimer, *J. Mol. Struct.*, 988, 24–34(2011).
doi:10.1016/j.molstruc.2010.11.064

Prabavathi, N., Nilufer, A., Krishnakumar, V. and Akilandeswari, L., Spectroscopic, electronic structure and natural bond analysis of 2-aminopyrimidine and 4-aminopyrazolo[3,4-d]pyrimidine: A comparative study, *Spectrochim. Acta Part A*, 96, 226–241(2012).
doi:10.1016/j.saa.2012.05.015

Prabavathi, N., Nilufer, A. and Krishnakumar, V., Quantum mechanical study of the structure and spectroscopic (FT-IR, FT-Raman, 13C, 1H and UV), NBO and HOMO–LUMO analysis of 2-quinoxaline carboxylic acid, *Spectrochim. Acta Part A.*, 92, 325–335(2012).
doi:10.1016/j.saa.2012.02.105

Prabavathi, N., Nilufer, A. and Krishnakumar, V., Spectroscopic (FT-IR, FT-Raman, UV and NMR) investigation, conformational stability, NLO properties, HOMO–LUMO and NBO analysis of hydroxyquinoline derivatives by density functional theory calculations, *Spectrochim. Acta Part A*, 114, 449–474(2013).
doi:10.1016/j.saa.2013.05.011

Prasad, M. V. S., Udaya Sri, N., Veeraiah, A., Veeraiah, V. and Chaitanya, K., Molecular structure, vibrational spectroscopic (FTIR, FT-Raman),UV-Vis spectra, first order hyperpolarizability, NBO analysis, HOMO and LUMO analysis, thermodynamic properties of 2,6-dichloropyrazine by abinito HF and density functional method, *J. At. Mol. Sci.*, 4 (1), 1-17(2013).
doi:10.1016/j.molstruc.2010.11.064

Sebastian, S. and Sundaraganesan, N., The spectroscopic (FT-IR, FT-IR gas phase, FT-Raman and UV) and NBO analysis of 4-Hydroxypiperidine by density functional method, *Spectrochim. Acta Part A.*, 75, 941–952(2010).
doi:10.1016/j.saa.2009.11.030

Sebastian, S., Sylvestre, S., Sundaraganesan, N., Amalanathan, M., Ayyapan, S., Oudayakumar, K. and Karthikeyan, B., Vibrational spectra, molecular structure, natural bond orbital, first order hyperpolarizability, TD-DFT and thermodynamic analysis of 4-amino-3-hydroxy-1-naphthalenesulfonic acid by DFT approach, *Spectrochim. Acta Part A.*, 107, 167–178(2013).
doi:10.1016/j.saa.2013.01.041